ETH zürich

ETH Library

Interdependencies between the distribution of density, land use, and the cost-effectiveness of district cooling systems

Working Paper

Author(s):
Shi, Zhongming; Fonseca, Jimeno A.; Schlueter, Arno

Publication date:
2020

Permanent link:
https://doi.org/10.3929/ethz-b-000391819

Rights / license:
In Copyright - Non-Commercial Use Permitted

This page was generated automatically upon download from the ETH Zurich Research Collection.
For more information, please consult the Terms of use.

Design of density and land uses for the cost-effectiveness of district cooling systems in high-density cities

Zhongming Shi [a, b, *], Jimeno A. Fonseca [a,b], Arno Schlueter [a,b]

[a] Future Cities Laboratory, Singapore-ETH Centre, 1 Create Way, CREATE Tower, Singapore 138602, Singapore
[b] Architecture and Building Systems, ETH Zurich, Stefano-Franscini-Platz 1, Zurich 8093, Switzerland

Abstract
Density and land uses are two fundamental components controlled in a city's master plan. Together, they affect both spatial and temporal distributions of the cooling demand in a district. This work studies how the design of density and land use impacts the cost-effectiveness of district cooling systems in high-density cities. To approach this, we take the street layout plan of Downtown Singapore and generate hundreds of designs of density and land uses using Grasshopper and the quasi-Monte Carlo Saltelli sampler. Five independent input variables are used for sampling. The three land uses featured are residential, office, and retail. We assess the cost-effectiveness for the district cooling systems in each sample with a simulation program called the City Energy Analyst. To determine the effects of various designs on the cost-effectiveness of the district cooling systems, we perform the Sobol' sensitivity analysis. We find that the District land use ratio followed by the spatial distribution of density has the dominant role, while the spatial distribution of land uses has a minor influence on the cost-effectiveness of district cooling systems. Urban planners and designers may use the results of this study in the design of density and land use for a district of high-density cities serviced by district cooling systems.

Keywords: floor area density; land use; district cooling systems; capital cost; operational cost; energy-driven urban design

Nomenclature

DCS	district cooling system
$CAPEX$	capital cost [USD]
$OPEX$	operational cost [USD]
$aCAPEX$	annualized capital cost-effectiveness [USD/MWh]
$aOPEX$	annual operational cost-effectiveness [USD/MWh]
CEA	City Energy Analyst
CH	chiller
CT	cooling tower

1. Introduction

The design of floor area density and land uses for each block is of great importance in the realm of urban planning and design. They define the gross floor area and building functions of a given block. Floor area density and land uses are often measured by floor area ratio and land use ratio. Floor area ratio equals the ratio of the gross building floor area in a block to the area of that block. Land use ratio equals the ratio between the gross floor areas of each land use type in a block. Figure 1 presents an example master plan with the floor area ratio illustrated in numbers and the land uses in colors (Urban Redevelopment Authority, 2014). At the block scale, the design of floor area density and land uses may affect the architectural design. For example, for blocks of the same high floor area ratio, the residential-dominated block may tend to have much slim building volume design for the purposes of natural sunlight accessibility. At a larger district scale, it adds another dimension to the design of floor area density and land uses - their inter-block relationships. The spatial distribution of the floor area ratio and land use ratios shapes the morphological cityscape. Also, it creates the flow of humans and all forms of traffic along the street or the utility networks. For example, the locations of job and home create the flows of commuters; the utility consumers with various needs and schedules affect the distribution of utilities.

Figure 1. Density and land use control in an exemplary master plan (Urban Redevelopment Authority, 2014).

In high-density cities, district cooling systems (DCS) which rely on a centralized cooling production are efficient means of cooling supply (UNEP, 2015). As shown in Figure 2, the basic components of a DCS include a district cooling plant (chillers and cooling towers), pumps, and a piping network. The piping network links the district cooling plant to its end-users. The DCS cost-effectiveness is associated with both the capital and the operational costs. The capital cost is determined by the sizing of each DCS component and the pricings. The operational cost includes that spent on the thermal loss and pressure drop in the distribution additional to that spent on the effective cooling supply. The peak thermal loss, though much lower than that in a district heating system, can surpass as much as 10% of the cooling supply (Li et al., 2017), while the pressure drop may contribute up to 10% of the total DCS electricity consumption (Guelpa et al., 2016; Li et al., 2017).

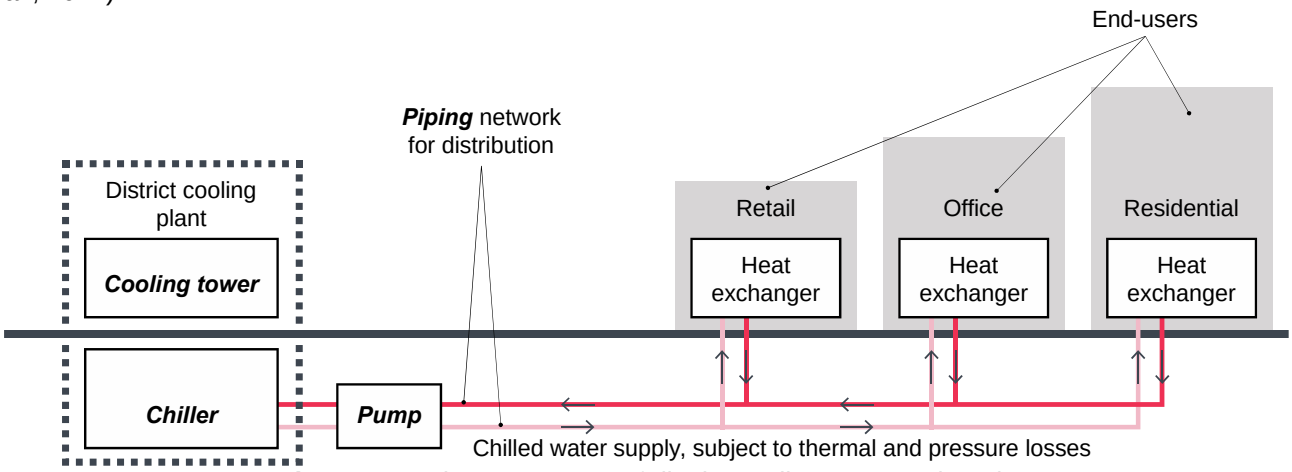

Figure 2. Basic components of district cooling systems (DCS).

For a district, the design of floor area density and land uses affects the DCS costs by affecting the spatial and temporal distributions of the cooling demand. Regarding capital costs, the sizing of each DCS component is based on the annual peak of the temporal distribution of the district's cooling demand. The peak can be affected by the building volume design for the solar radiation received (Cheng et al., 2006) or the cooling demand profiles of various land uses aggregated. Regarding operational costs, the thermal loss

comes in the form of conductive and convective of heat transfer (Keçebaş et al., 2011). They are affected by the distance that the chilled water needs to travel and pipe diameters, respectively (Bergman et al., 2017). The pressure drop is affected by the mass flow, pipe length and diameter (Rogenhofer, 2018). All these factors are directly related to the spatial and temporal distributions of the district's cooling demand. Figure 3 summarizes the interdependencies between the design of floor area density, land uses and the affected capital and operational costs of district cooling systems.

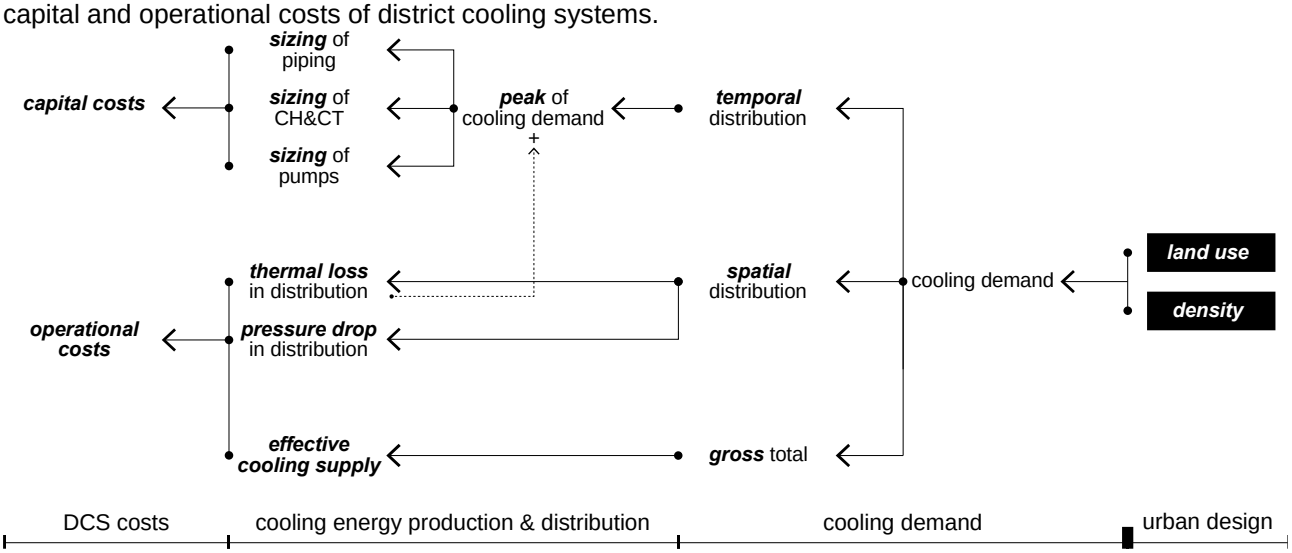

Figure 3. Links between urban density, land use, and DCS capital and operational costs. Chillers and cooling towers are denoted as CH and CT, respectively.

1.1. State-of-the-art

1.1.1. Related works and the knowledge gap

Studies on the interdependencies between urban design and energy efficiency fall into either category of the passives and the actives (Shi, Fonseca, et al., 2017b). The passives focus on manipulating the urban design parameters for energy demand reductions. In contrast, the actives focus on adjusting the urban design parameters to improve the efficiency of urban energy systems, like the district cooling systems. Compared to the extensive research performed for the passives, fewer have touched the actives. Among them, some dedicate to the interdependencies between various performance metrics of the district thermal networks and the design of floor area density and land uses. Table 1 summarizes these recent related studies (Best et al., 2015; Cajot et al., 2016; Chow et al., 2004; Fonseca et al., 2017; Yan et al., 2017) by the performance metrics and the two aspects (overall quantity and spatial distribution) of the design of floor area density and land uses.

Table 1. A summary of recent studies on the design of density, land use, and the performance of district thermal systems. V stands for input variables; C stands for constants; and X stands for not discussed.

Performance metrics	**Floor area density** (Overall quantity)	**Floor area density** (Spatial distribution)	**Land uses** (Overall quantity)	**Land uses** (Spatial distribution)	**References**
Cooling demand fluctuation	C	X	V	X	(Chow et al., 2004)
Annualized capital costs; greenhouse gas emissions	C	X	V	X	(Best et al., 2015)
Greenhouse gas emissions; electricity consumption	V	X	V	X	(Fonseca et al., 2017)
System Coefficient of Performance, or electricity consumption	C	X	V	X	(Yan et al., 2017)
Annualized capital costs; annual operational costs	C	V	V	V	(Cajot et al., 2016)

Table 1 reveals that the knowledge gap mainly lies on the interdependencies between the performance of district thermal networks and the spatial distributions of floor area density and land uses. However, we realize that Cajot et al. attentively established a potential link regarding this knowledge gap (Cajot et al., 2016). The performance metrics used were annualized capital and annual operational costs of the district thermal system. One advantage of using the monetary costs as the performance metrics is that they provide a common ground for comparing the affected aspects including the sizings of the components, thermal loss, and pressure drop. Unfortunately, they did not further elaborate on these links for quantified interdependencies or urban design suggestions. Also, their model of district thermal systems used the direct linear distances between the centralized plant and end-users instead of the actual routes of the piping network, which usually follows the street layout. This over-simplification ignores the potential thermal loss and pressure drop in the actual routes of chilled water distribution and, thus, hurts the reliability of their results.

1.1.2. Experimental design method

Sensitivity analysis identifies the importance of a model's input variables on the variability of its outputs (Yan et al., 2017). It has been widely used in studies on the interdependencies between building design and building energy performance (Tian, 2013). Sensitivity analysis methods use either local or global techniques. Local sensitivity analysis concentrates on the importance of a single input variable while keeping the other parameters fixed (Kristensen & Petersen, 2016). The results of Local sensitivity analysis can be misleading if the model is of unknown linearity (Delgarm et al., 2018). In contrast, Global sensitivity analysis produces robust results in the presence of non-linearity. It also considers the interactions between multiple input variables and tests their simultaneous effects on the model's outputs. Morris Method (Morris, 1991) and Sobol' method (Sobol′, 2001) are commonly used Global sensitivity analysis methods for investigations on building energy performance (Kristensen & Petersen, 2016). Morris method is able to identify the important input variables and produce a ranking by their importance. Sobol' method even quantifies the importance of the input variables with two levels of effect indices. However, the main disadvantage of the Global sensitivity analysis is the high computational cost (Delgarm et al., 2018). One can adopt an efficient quasi-Monte Carlo sampling technique; simulate a small number of samples and apply a predictive model to amplify simulated dataset; or use fast simulation tools (Shmueli et al., 2017; Tian, 2013).

To generate large-number samples of urban geometries for the sensitivity analysis, Grasshopper on Rhino 3D (Robert McNeel & Associates, 2019) is a popular choice of tool (Natanian et al., 2019; Zhang et al., 2019). Grasshopper offers a user-friendly visual programming platform for parametric design modeling. It helps produce thousands of design scenarios based on the combinations of given design parameters within seconds. Also, Grasshopper provides the possibilities of tool coupling. Through a connection to any simulation tool of performance assessment, it expands Grasshopper's capabilities to facilitate the analytical design workflow.

1.1.3. Assessment tools

A suitable simulation program for the sensitivity analysis should be able to forecast a district's cooling demand, size the DCS' chillers, cooling towers, pumps, and piping networks, as well as simulate the pressure drop and the thermal loss in distributing the chilled water. These intermediate results are needed for calculating the affected DCS costs and DCS cost-effectiveness indicators (Details in Section 2.4.3). An open-source toolbox named the City Energy Analyst (CEA) meets these requirements. It performs building energy modeling at the district scale (Fonseca et al., 2016). The CEA simulations are performed on hourly-basis over a year of 8,760 hours. With a connection to a parametric geometric urban design model in Grasshopper, CEA is able to automate large-number iterations of energy simulations for the sensitivity analysis. Examples of energy simulation tools include the Ladybug and Honeybee (Roudsari & Pak, 2013) and the Rhino-based Urban Modeling Interface (umi) (Reinhart et al., 2013). Both tools can forecast the cooling demand for a given scenario of urban design. However, neither of them is able to design the DCS. Letellier-Duchesne et al. built an extension to the demand simulation module of umi (Letellier-Duchesne et al., 2018). Similar to CEA, it is able to perform district thermal system design and optimization for costs, carbon dioxide emissions, etc. Though very promising, the current version of this extension is not yet capable of calculating any thermal loss in the distribution network (Letellier-Duchesne & Nagpal, 2017).

1.2. Contributions

This paper aims at the bridging the knowledge gap discussed in Section 1.1.1. The main contributions of this research are summarized as follows. (1) Model integration. We integrate a model for the design of floor area density and land uses with a detailed engineering model for urban energy system design and assessment.

Links of high granularity between urban design including the spatial distributions of floor area ratio, land use ratios and the sizing of DCS components, thermal loss, and pressure drop are to be established. In addition, to compare the weights of these links, we measure the affected aspects of DCS in the form of monetary costs. In this way, the model is able to answer research questions like: to what extent, do the design of floor area density and land uses affect the various aspects of DCS cost-effectiveness? (2) Insights for energy-driven urban design. We target at providing urban designers with insights for answering questions like: how to design the floor area density and land uses for a cost-effective DCS, at the early stage of urban design processes? These insights can be used at the early stages of urban design for a high-density urban district serviced by a DCS. To approach this, we further the established links for quantified active interdependencies. (3) Metrics for spatial distributions of floor area density and land uses. Being parsimonious to the number of input variables for less computational expenses, we introduce the concept of Density gradient and Land use gradient to describe the spatial distributions of floor area ratios and land use ratios. Their calculations are detailed in Section 2.2.2 and Section 2.2.3.

We structure the paper as follows. In Section 2, we detail the methods to approach the two research questions using Downtown Singapore as an example. The results are presented and explained in Section 3. Then, we extend a discussion in Section 4 and finally, conclude the findings in Section 5.

2. Methods

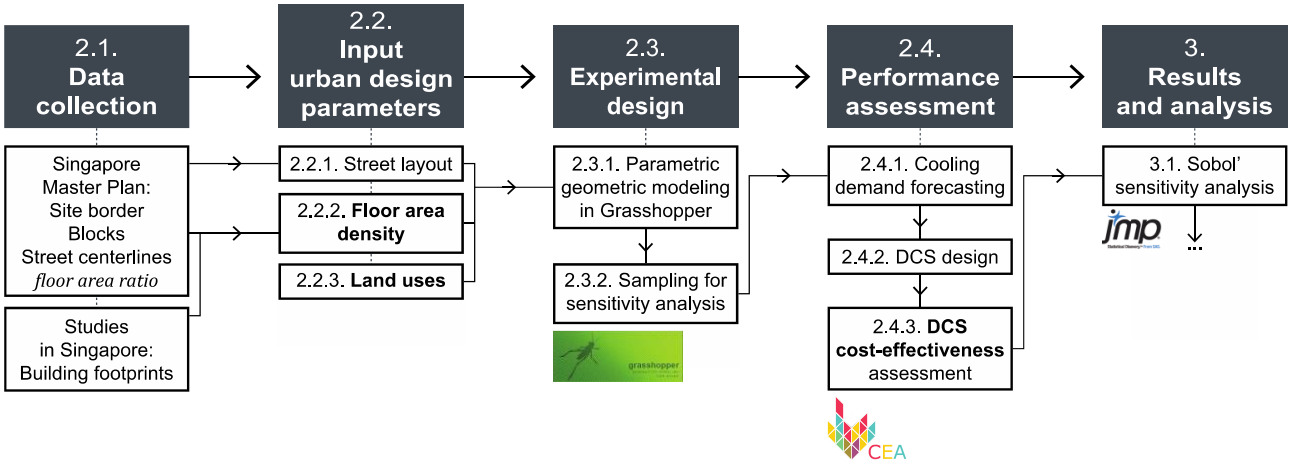

Figure 4. The five-step workflow and the tools used in this study.

The methodological framework of this work has a five-step workflow as presented in Figure 4. The first four steps are detailed in this section and the fifth step is presented in Section 3. Section 2.1 describes the sources of data used. Section 2.2 describes the input variables of the experiments after preprocessing. Section 2.3 describes the method used for the experimental design. Finally, Section 2.4 describes the tool (City Energy Analyst) used for performance assessment on the DCS cost-effectiveness.

2.1. Data collection

Figure 5. The location of the case study at Downtown Singapore and the Singapore Master Plan 2014.

We gather GIS data about the floor area ratio for each block in the selected district of Downtown Singapore (Figure 5). These data are retrieved from the Singapore Master Plan (2014) (Urban Redevelopment Authority, 2014). We use them to set the boundary conditions of our study. By doing so, we limit the variations of the input design variables within the development framework envisioned by the local planning authority of Singapore. Besides, we extract the street layout in the district. However, the Singapore Master Plan has little data available regarding the building footprints, as this district is in planning yet with few occupying buildings. We extract these missing data about the building footprints and their site coverage from a study on urban geometries in the high-density areas of Singapore (Shi et al., 2019).

2.2. Input urban design parameters

This subsection serves to introduce the input variables and parameters that build up the parametric geometric model for the sampling of sensitivity analysis in Grasshopper.

2.2.1. Street layout and blocks

We use the data of Section 2.1 to extract the centerlines of all the street segments (between intersections) and the borderlines of all the blocks in the selected district of Downtown Singapore. The layout of the DCS piping network follows these centerlines. All buildings are contained inside these borderlines.

2.2.2. Floor area density

We use Density gradient to measure the spatial distribution of floor area density (floor area ratio). In this work, Density gradient describes the proximity of high or low floor area ratio to the DCS cooling plant. As in Equation 1 and Figure 6, the Density gradient equals the difference in floor area ratio between the furthest ($\boldsymbol{f}$) and the closet ($\boldsymbol{p}$) block to the DCS cooling plant divided by the Route distance between these two blocks. The Route distance between two nodes on a piping network measures the total length of all pipe segments connecting these two nodes. The floor area ratio for each block ranges between 3 and 25, based on the minimum requirement for a block to be qualified as high-density and the highest floor area ratio found in the Singapore Master Plan (Urban Redevelopment Authority, 2014). The longest Route distance found in the district of study is ~1,010 m. In consequence, the lower and upper limits of the Density gradient are set between ± (25-3)/1010 = ± 0.02718 m^{-1}. Within this range, when all the blocks serviced by the DCS cooling plant have the same floor area ratio, the Density gradient equals zero. Otherwise, when the Density gradient is above (below) zero, the blocks nearer to the DCS cooling plant will have a higher (lower) floor area ratio.

$$Density\ gradient = \frac{Floor\ area\ ratio_p - Floor\ area\ ratio_f}{Route\ distrance_f} \quad (1)$$

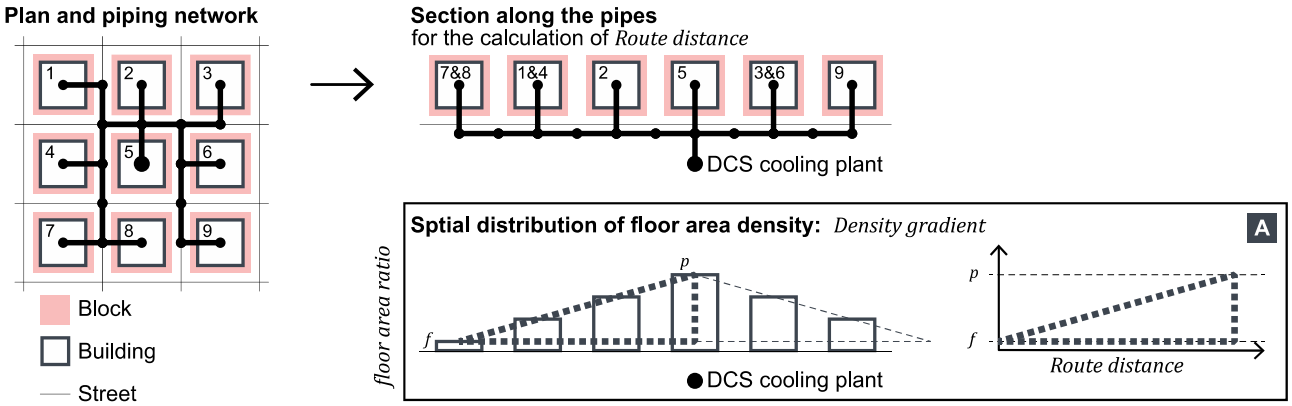

Figure 6. Route distance [m], Density gradient [m^{-1}], and their calculations. The point closest and furthest to the DCS cooling plant is denoted as $\boldsymbol{p}$ and $\boldsymbol{f}$, respectively.

Throughout this work, the district's gross floor area remains constant at ~5,000,000 sqm, envisioned by the local planning authority in the Master Plan (Urban Redevelopment Authority, 2014). Also, each block contains one building with the site coverage set at 0.47. The building footprint follows a podium building pattern, which is offset by the block's borderline. These settings for the buildings are based on the average site coverage and the most dominant building pattern of the 178 blocks surveyed in the high-density areas of Singapore (Shi, Hsieh, et al., 2017). Together with a given Density Gradient, the floor area ratio and the gross floor area for each of the n blocks in the district can be calculated with Equation 2 and Equation 3.

$$Floor\ area\ ratio_n = \frac{5000000sqm - \sum_{b=1}^{n}(1010m - Route\ distance_b) \times Density\ gradient \times Block\ area_b}{\sum_{b=1}^{n} Block\ area_b} + (1010 - Route\ distance_n) \times Density\ Gradient \quad (2)$$

$$Gross\ floor\ area_n = Floor\ area\ ratio_n \times Block\ area_n \quad (3)$$

2.2.3.Land uses

Three land uses - residential, office, and retail - are used in this study as they are usually the most common and dominant land uses in high-density cities. Two variables - Residential gradient and Office gradient - are used to measure the spatial distribution of residential and office land uses. As in Figure 7 and Equation 4, Residential gradient and Office gradient are calculated with a similar method as that of the Density gradient. Land use gradient equals the difference in land use ratio between the furthest ($\boldsymbol{f}$) and the closet (p) block to the DCS cooling plant divided by the Route distance between these two blocks. The land use ratio of the block furthest from the DCS cooling plant is named as the Initial land use ratio. Initial residential ratio and Initial office ratio are used as input variables in addition to Residential gradient and Office gradient. As land use ratios range between 0 and 1, the lower and upper limits of the two Land use gradients are set between ± (1-0)/1010 = ± 0.00099 m^{-1}. Also, the Initial residential ratio and Initial office ratio are set between 0 and 1.

$$Land\ use\ gradient = \frac{Land\ use\ ratio_p - Land\ use\ ratio_f}{Route\ distrance_f} \quad (4)$$

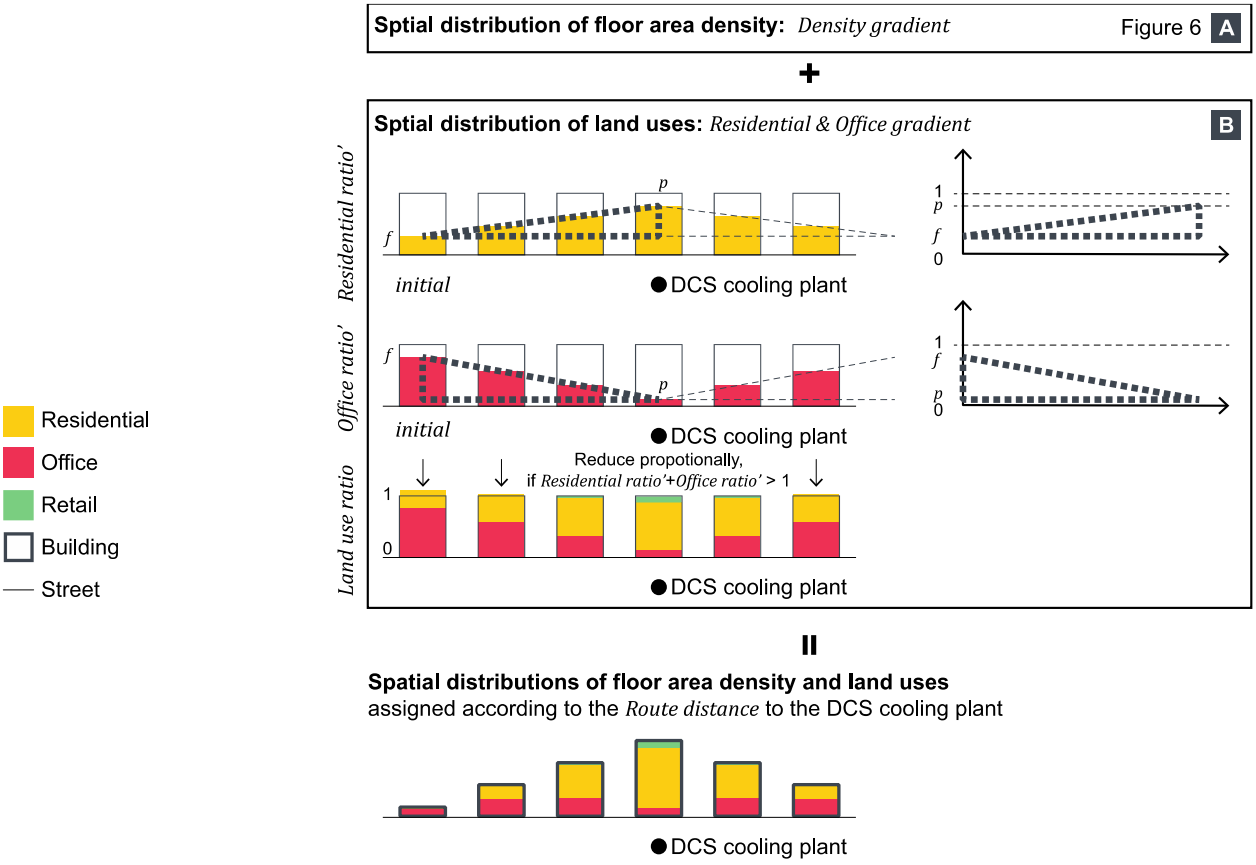

Figure 7. Residential gradient [-], Office gradient [-], Retail ratio [-], District land use ratio [-], and their calculations. The point closest and furthest to the DCS cooling plant is denoted as $\boldsymbol{p}$ and $\boldsymbol{f}$, respectively.

With all four input variables on land uses, the Residential ratio and Office ratio of each of the n blocks in the district are calculated with Equation 5. Need to notice, when the sum of residential ratio and office ratio is

larger than 1, both of them have to be proportionally reduced until their sum equals 1, as in Figure 7, Equation 6, and Equation 7. The Retail ratio of each block is calculated as 1 subtracted by the sum of the Residential ratio and Office ratio, as in Equation 8. Also, the share of each land use type over the district's gross floor area is named as the District land use ratio. Table 2 summarizes the major urban design parameters mentioned so far and the five independent input variables are indicated.

$$Land\ use\ ratio'_n = Initial\ land\ use\ ratio_p + Land\ use\ gradient \times (1010m - Route\ distance_n) \quad (5)$$

$$Residential\ ratio_n = \frac{Residential\ ratio'_n}{\max(1, Residential\ ratio'_n + Office\ ratio'_n)} \quad (6)$$

$$Office\ ratio_n = \begin{cases} Office\ ratio'_n,\ if\ Residential\ ratio'_n + Office\ ratio'_n \leq 1 \\ 1 - Residential\ ratio_n,\ if\ Residential\ ratio'_n + Office\ ratio'_n > 1 \end{cases} \quad (7)$$

$$Retail\ ratio_n = 1 - (Residential\ ratio_n + Office\ ratio_n) \quad (8)$$

Table 2. A summary of the major urban design parameters involved.

Design parameters	Variables	Boundary	Definition/calculation
Floor area ratio [-]	-	[3, 25]	Ratio of gross floor area in a block/district to the area of that block/district
Density gradient [m^{-1}]	V	[± 0.02718]	See Equation 1
Land use ratio [-]	-	[0, 1]	Ratio between the floor area of each land use type in a block
Route distance [m]	-	[0, 1010]	See Figure 6
Residential gradient [m^{-1}]	V	[± 0.00099]	See Equation 4
Office gradient [m^{-1}]	V	[± 0.00099]	See Equation 4
District land use ratio [-]	-	sum = 1	Ratio between the gross floor area of each land use type in the district
Initial residential ratio [-]	V	[0, 1]	The residential land use ratio of the block furthest by Route distance from the district cooling plant
Initial office ratio [-]	V	[0, 1]	Same as above

2.3. Experimental design

2.3.1.Parametric geometric modeling in Grasshopper

Based on the five independent inputs variables and other input parameters detailed in Section 2.2, we build the parametric geometric model of the district in Grasshopper. The model coupled with the City Energy Analyst (CEA) allows the iteration of urban form generation, energy simulations, and performance assessment for the sensitivity analysis. Figure 8 provides two examples of the district generated by this parametric geometric model in Grasshopper. These two examples show how the design of floor area density and land uses is manipulated by the five independent input design variables.

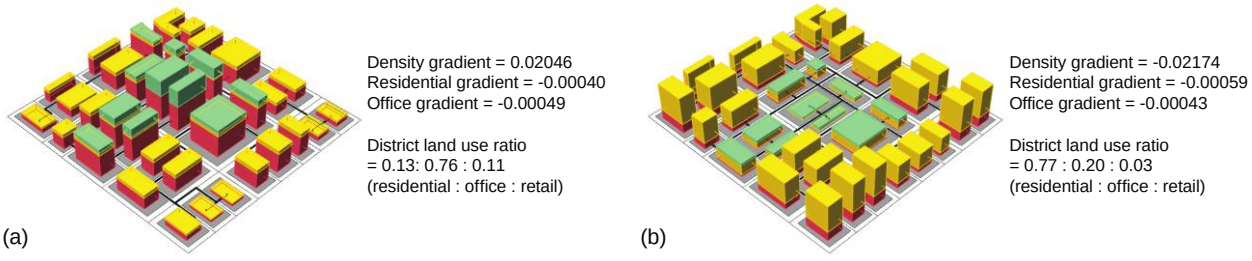

Figure 8. Two examples of the district generated by the parametric geometric model in Grasshopper.

2.3.2. Sampling for the sensitivity analysis

The Sobol' sensitivity analysis is of heavy computational expenses as it requires thousands of samples to converge. It takes up to six hours to complete a full performance assessment for each sample with the City Energy Analyst (CEA). To reduce the computational expenses, we adopt a quasi-Monte Carlo sampler (Saltelli et al., 2010) using SALib (Herman & Usher, 2017) and an artificial neural network to amplify the

number of the simulated samples with JMP Pro 13 (SAS Institute Inc., 2016). First, following the recommendations of (Herman & Usher, 2017), the sample size is set at N = 35 making a total number of $N \cdot (2k+2)$ = 420 samples, where k equals 5 (the number of input variables). Figure 9 illustrates the probability density function of the sampled values for the five independent input variables. Second, using these sampled input variables, we use the parametric geometric model built in Section 2.3.1 to generate the urban geometries and then execute the performance assessment with CEA. Next, we use the simulated results to inform the artificial neural network that propagates the size of the dataset for the sensitivity analysis.

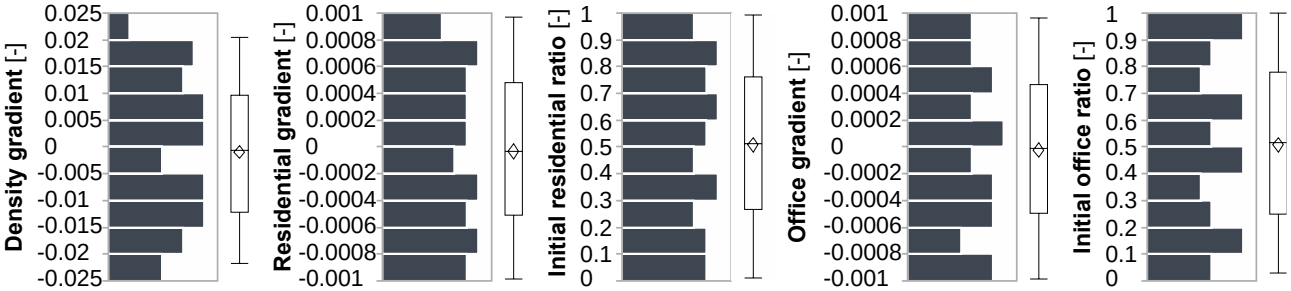

Figure 9. Distribution of the sampled values for the five input variables, Density gradient [-], Residential gradient [-], Initial residential ratio [-], Office gradient [-], and Initial office ratio [-].

Artificial neural networks have been widely utilized in solving predictive problems for studies on building energy efficiencies (Mohandes et al., 2019). Though not yet with a focus on the DCS cost-effectiveness, it has been used in studies involving various metrics of urban development (Silva et al., 2018). An artificial neural network consists of three layers - the input layer, the hidden layer, and the output layer. The relationships between the inputs and the outputs are decided by an activation function. For building energy studies, Linear Function and Hyperbolic Tangent Function are the commonly used activation functions (Mohandes et al., 2019). KFold crossvalidation is used to avoid the artificial neural network's tendency to overfit the data (Shmueli et al., 2017). It subdivides a dataset into K subsets. Each of the subsets rotates to serve to validate once as the other K-1 subsets all have served to train the model of prediction. After a series of rounds of trials for the number of neurons, hidden layers, and KFold as well as the activation function, the best R square and mean absolute deviation are witnessed using the following settings. One hidden layer and 5 neurons with the Hyperbolic Tangent Function are used and the number of KFold is set at 5. R square (the coefficient of multiple determination) and the Mean absolute deviation are commonly used as the indicators for prediction accuracy (Mohandes et al., 2019). The R square and the mean absolute deviation achieved in this work are presented in Table 5 and their interpretations are detailed in Section 3.1.

2.4. District cooling systems design and assessment

We use the CEA v2.9.2 for the cooling demand forecasting, district cooling systems (DCS) design, and the performance assessment (The CEA team, 2019).

2.4.1. Cooling demand forecasting

The cooling demand forecasting provides the inputs for the DCS design, simulation, and performance assessment. It is conducted for each iteration with the inputs including the building geometries and their spatial locations, as well as the occupancy types (land uses). They all come from the parametric geometric model in Section 2.3. Other inputs including the ratio of air-conditioned area, the temperature set points, the HVAC technology selection for each DCS component, the properties of the building envelope, the weather conditions in Singapore are from the CEA v2.9.2 database (The CEA team, 2019). CEA uses a space-based occupant behavior modeling approach (Happle et al., 2018). The occupancy schedules are adjusted from ASHRAE standard schedules (ASHRAE Project Committee 90.1., 2019). The output of cooling demand forecasting is the hourly cooling demand of each building for the 8,760 hours of a year.

2.4.2. District cooling systems design

Piping network design

In this study, we have the piping network of a DCS follow the street layout. Its connection to each end-user is located at the centroid of the building. The cooling plant located in the centroid of the entire district. The piping network design used in all iterations is illustrated in Figure 10. It has the shortest total length of all pipe segments. Branched layouts without loops are used. The piping network layout is determined using the

Steiner spanning tree algorithm (Cormen et al., 2009) implemented in the CEA v2.9.2 (The CEA team, 2019).

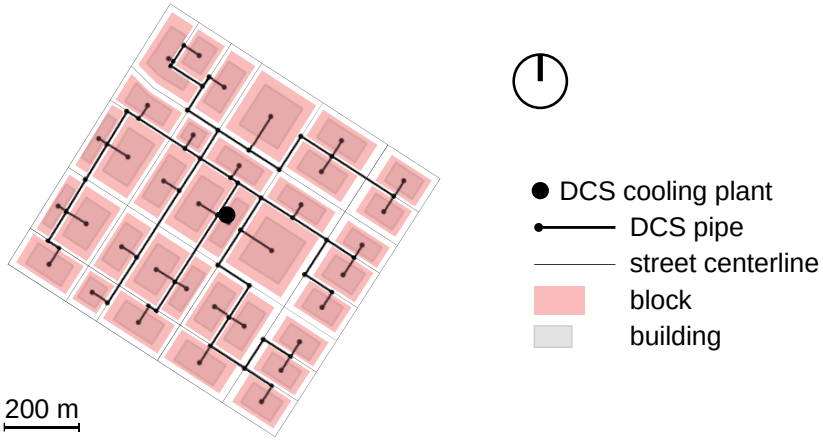

Figure 10. The piping network layout used in all iterations.

Chilled water production and distribution

Besides cooling demand and piping network, this step requires a series of other parameters concerning the simulations of chilled water production and distribution (Table 3). In all 420 iterations, the technology selections for each DCS component are kept the same. The DCS cooling plant comprises of vapor compression chillers and cooling towers, the sizes of which are decided based on the peak cooling demand and the thermal loss in the piping network. The pipe diameter of each segment of the piping network is decided based on the peak mass flow rate. The size of pumps is decided based on the peak pressure drop along the piping network.

Table 3. DCS Input parameters in this study

Parameter	Value	Unit	Note
Thermal conductivity of polyurethane	0.023	W/mK	-
Supply Temperature in DCS networks	~5.4	°C	-
Plant COP	~4.4	-	Including operation of all devices at the cooling plant

2.4.3.Performance assessment

To compare across samples with various sizes of district's annual cooling demand, we use the following five metrics as the DCS cost-effectiveness indicators. They are the annualized capital costs on the piping, chillers & cooling towers, and pumps, as well as the annual operational cost on thermal loss and pressure drop divided by the annual effective cooling supply. The DCS cost-effectiveness indicators of annualized capital costs are calculated from the capital costs using Equation 9, where i stands for the interest rate; n stands for the estimated lifetime (25 years for all technologies, except for 20 years for the cooling towers); qc stands for the district's annual effective cooling supply that equals the district's annual cooling demand. The capital costs of the pipes, cooling plants, and pumps are based on their required sizes and the technology pricings stored in the CEA database (The CEA team, 2019). The annual operational costs are calculated based on that spent on the electricity consumed for compensating the thermal loss and overcoming the pressure drop. The marginal electricity price used in this study is 0.15 USD/KWh (Energy Market Authority, 2018). The five DCS cost-effectiveness indicators are denoted as $aCAPEX_{piping}$, $aCAPEX_{CH\&CT}$, $aCAPEX_{pump}$, $aOPEX_{qloss}$, and $aOPEX_{\Delta p}$.

$$aCAPEX_{technology} = \frac{CAPEX_{technology} \cdot \frac{i(1+i)^n}{(1+i)^n-1}}{qc} \quad (9)$$

3. Results and analysis

3.1. Sobol' sensitivity analysis

The two levels of effect indices in Sobol' sensitivity analysis are the Main effect (or the First-order effect) and the Total effect. The Main effect quantifies the impacts of the input variables independently, while the Total effect considers the interactions between the input variables including the First-order effect and all higher-

order effects (Petersen et al., 2019). In this work, we mainly look at the Total effect. Table 4 displays the Total effects in the Sobol' sensitivity analysis with the predicted dataset by the artificial neural networks in JMP pro 13. Table 5 shows R square and mean absolute deviation of the artificial neural network as well as the minimum and the maximum values of each DCS cost-effectiveness indicator's simulated dataset. With an R square above or close to 0.9, the model of artificial neural networks produces reliable predicted datasets for the three DCS cost-effectiveness indicators of piping, chillers and cooling towers, and thermal loss. The Mean absolute deviation describes that the predicted dataset has only an average of difference at 0.004, 0.119, and 0.006 USD/MWh from the simulated dataset for the three indicators, respectively.

Table 4. Total effects [-] of the five input variables on the five DCS cost-effectiveness indicators.

	$aCAPEX_{piping}$	$aCAPEX_{CH\&CT}$	$aCAPEX_{pump}$	$aOPEX_{qloss}$	$aOPEX_{\Delta p}$
Density gradient	**0.268**	0.014	0.443	0.011	0.329
Residential gradient	0.032	0.032	0.175	0.028	0.054
Initial residential ratio	**0.699**	**0.7**	0.049	**0.94**	0.258
Office gradient	0.005	0.034	0.057	0.002	0.056
Initial office ratio	**0.109**	**0.345**	0.377	**0.124**	0.258

Table 5. The R square [-] and the mean absolute deviation [USD/MWh] of the artificial neural network, as well as the minimum and the maximum values [USD/MWh] in the simulated dataset.

	$aCAPEX_{piping}$	$aCAPEX_{CH\&CT}$	$aCAPEX_{pump}$	$aOPEX_{qloss}$	$aOPEX_{\Delta p}$
R square	0.96	0.89	0.54	0.97	0.85
Mean absolute deviation	0.004	0.119	0.013	0.006	0.01
Max. in simulated dataset	0.23	7.73	0.37	0.03	0.41
Min. in simulated dataset	0.13	4.49	0.23	0.01	0.16

For the three DCS cost-effectiveness indicators of piping, chillers and cooling towers, and thermal loss in Table 4, two preliminary observations are made as follows. The first observation regards the four input variables on the design of land uses. Among them, Residential gradient and Office gradient are more related to the spatial distribution of the cooling demand within the district, while Initial residential ratio and Initial office ratio are more related to the cooling demand's temporal distribution over a year. Based on the Sobol' sensitivity analysis indices, it appears that the cooling demand's temporal distribution is much more influential than its spatial distribution. The urban design parameter directly associated with the district's temporal distribution of cooling demand is the District land use ratio. The second observation regards the Density gradient that is related to the design of floor area density. It only presents an obvious impact on the DCS cost-effectiveness indicator of piping.

3.2. Five DCS cost-effectiveness indicators

In Figure **11**, we plot the five DCS cost-effectiveness indicators and the annual operational cost on the effective cooling supply at a uniform scale. Across the simulated dataset, the latter remains constant at 33.78 USD per MWh. The sum of the five DCS cost-effectiveness indicators accounts for up to ~27% of the sum of the six. Also, each of the five DCS cost-effectiveness indicator's contribution varies. The indicator of chillers and cooling towers dominates while the shares of the other are minor. However, when compared individually, the difference between the minimum and the maximum of each indicator ranges from ~60% for that on pumps to ~173% for that on thermal loss.

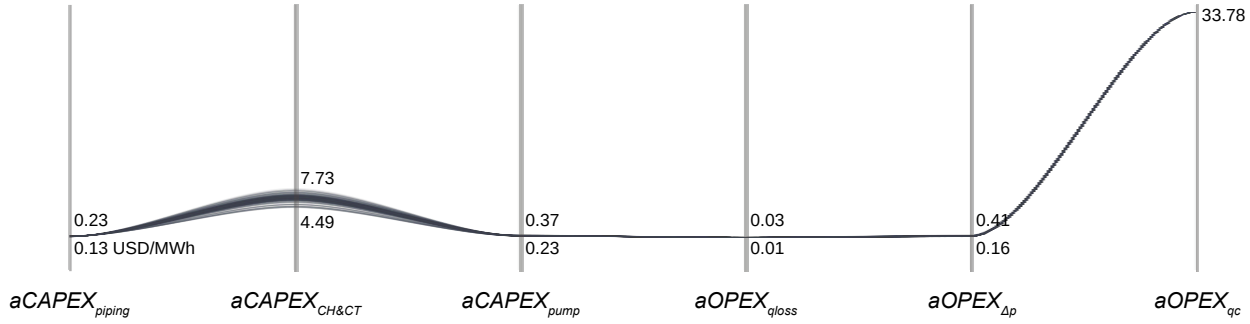

Figure 11. The five indicators of DCS cost-effectiveness plus the annual operational cost on the effective cooling supply per MWh, denoted as $aOPEX_{qc}$ [USD/MWh] at a uniform scale.

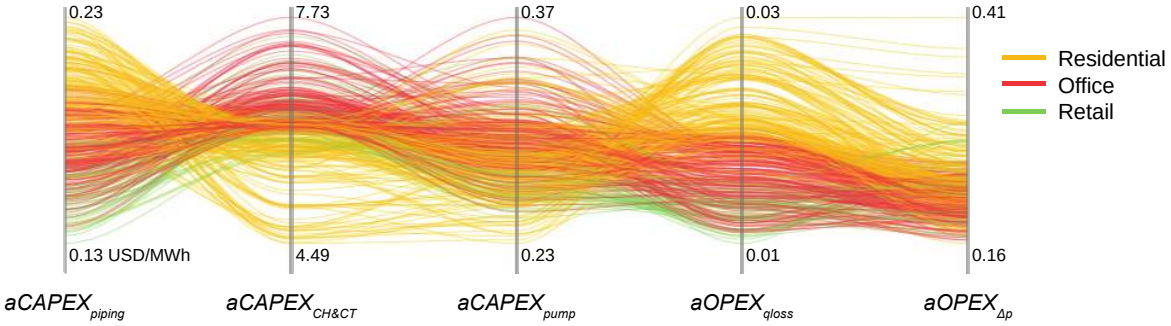

Figure 12. The five DCS cost-effectiveness indicators color-coded by the dominant land use of residential, office, and retail [USD/MWh] at a non-uniform scale.

In Figure **12**, we plot the five DCS cost-effectiveness indicators at a non-uniform scale. When color-coded by the dominant (≥50%) land use, the parallel plot reveals the following two trends. First, samples dominated by office and retail uses behave similarly. Second, trade-offs exist among the five DCS cost-effectiveness indicators. The office and retail-dominated samples behave in opposite to the residential-dominated ones for the indicators of piping, chillers and cooling towers, thermal loss, and pressure drop. For example, a high District residential ratio hurts the indicators of piping, thermal loss, and pressure drop, while favors the indicator of chillers and cooling towers. However, no obvious trends are revealed when the parallel plot is color-coded by the design variables on the spatial distributions of floor area density and land uses. In the following subsections, we aim for quantified interdependencies between the relevant design variables and the five indicators, individually.

3.2.1. Chillers and cooling towers

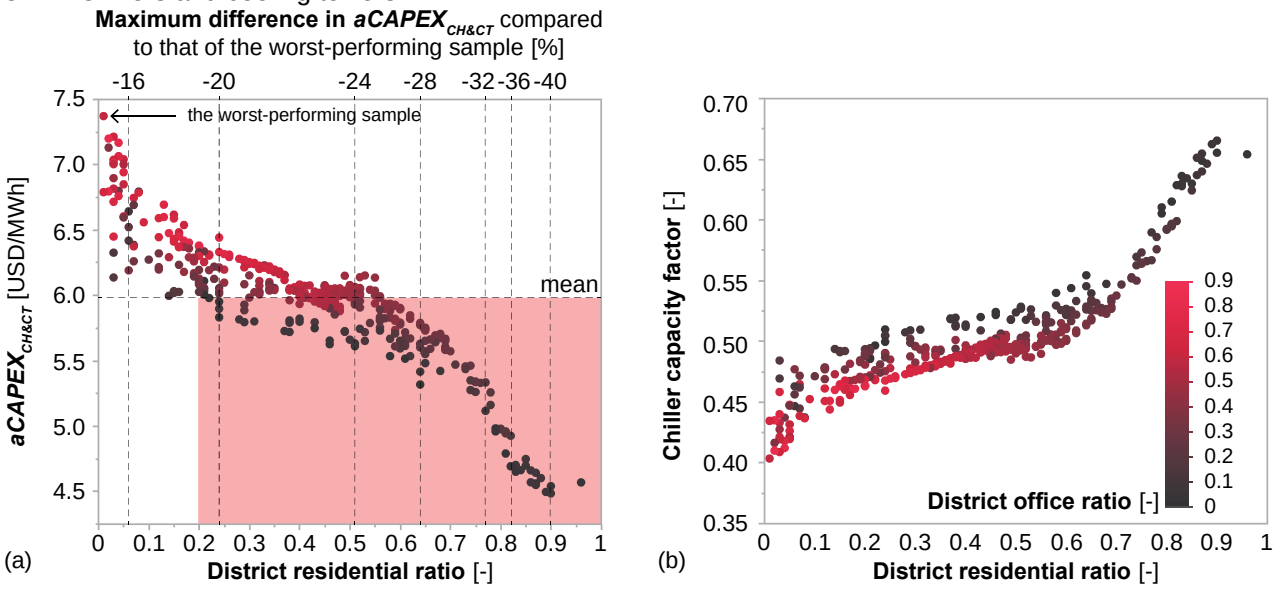

Figure 13. DCS cost-effectiveness indicator of chillers and cooling towers, denoted as $\boldsymbol{aCAPEX_{CH\&CT}}$ [USD/MWh] and Chillers capacity factor [-] by District residential ratio [-] and District office ratio [-].

In Figure 13(a), the DCS cost-effectiveness indicator of chillers and cooling towers improves as the District residential ratio increases. The rate of improvement plateaus when the District residential ratio is between ~0.20 and ~0.60. This plateau enables more flexibility for various combinations of District land use ratios. Though a high (>0.60) District residential ratio may significantly improve the DCS cost-effectiveness, the possibility for a mixed-use design is undermined in the meantime. Moreover, for the samples with the same District residential ratio, a relatively lower District office ratio tends to favor the DCS cost-effectiveness. To explain all these behaviors, we use the capacity factor of the chillers and plot it in Figure 13(b). The capacity factor equals the ratio of actual chilled water generated divided by the maximum chilled water generated if the system continuously functions at its nominal capacity over the same period of time (Equation 10). The land use combinations of the samples shaded in Figure 13(a) maintain the capacity factor above ~0.50 that keeps the indicator of chiller and cooling towers below its mean in the simulated dataset.

$$Capacity\ factor_{chiller} = \frac{Annual\ cooling\ energy\ generated}{365\ days \cdot 24\ hours/day\ \cdot\ Nominal\ capacity} \quad (10)$$

3.2.2.Piping network

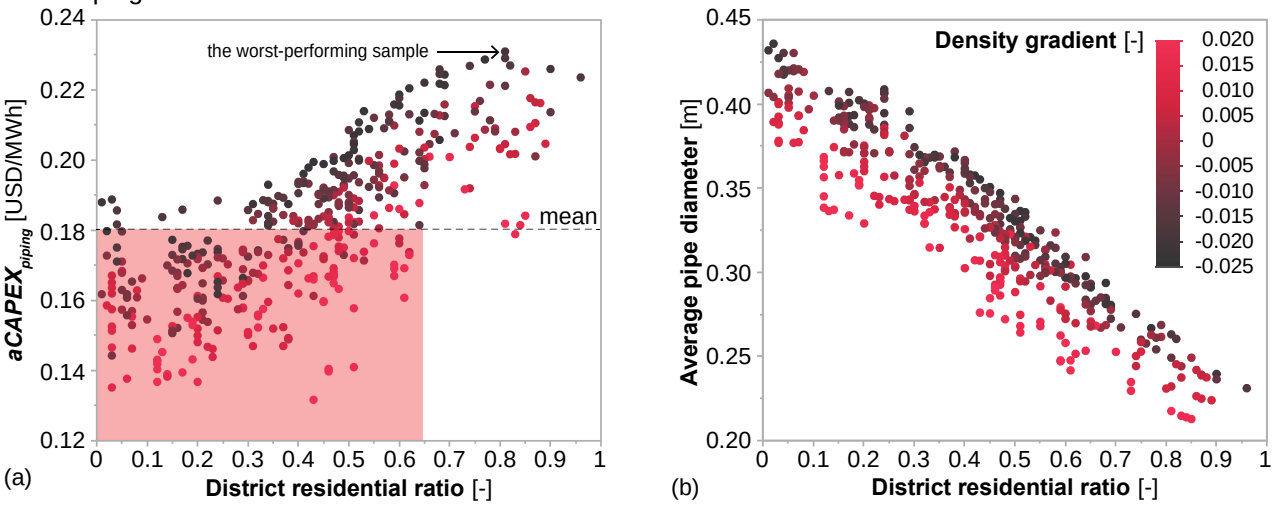

Figure 14. DCS cost-effectiveness indicator of piping, denoted as $\boldsymbol{aCAPEX_{piping}}$ [USD/MWh] by overall residential ratio [-] and Density gradient [-].

In Figure 14(a), the DCS cost-effectiveness indicator of piping generally improves as the District residential ratio decreases. This trend confirms its trade-off with the indicator of chillers and cooling towers. To explain this, we use the average diameter of all pipe segments and the pricings, as the length of each pipe segment remains the same. Figure 14(b) shows that samples with higher District residential ratio tend to have thinner pipes. The unit price of thinner pipes is higher than that of thicker ones. Thus, high District residential ratio using thinner pipes presents reduced DCS cost-effectiveness. Moreover, for the samples with the same District residential ratio, a higher Density gradient tends to improve the DCS cost-effectiveness. This means that having a higher floor area density in proximity to the DCS cooling plant improves the DCS cost-effectiveness on the piping network. The improvement can be as much as ~35%. This is because high Gradient density reduces the amount of chilled water to be distributed to the further side of the piping network. In this way, the need for installing thicker and pricier pipes at the further side of the piping network is reduced. The District residential ratios of the samples shaded in Figure 14(a) that with a high Density gradient keep the indicator of piping below its mean in the simulated dataset.

3.2.3. Thermal loss

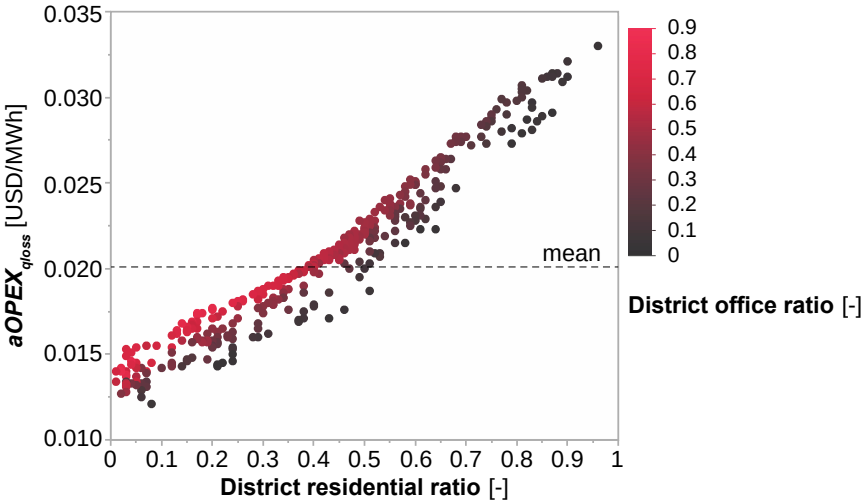

Figure 15. DCS cost-effectiveness indicator of thermal loss, denoted as $\boldsymbol{aOPEX_{qloss}}$ [USD/MWh] by District residential ratio [-] and District office ratio [-].

In Figure 15, the DCS cost-effectiveness indicator of thermal loss improves as the District residential ratio and District office ratio decreases. This trend confirms its trade-off with the indicator of chillers and cooling towers. The reason is that samples with higher District residential ratio are equipped with thinner pipes (see Figure 14(b)), and thinner pipes lead to more thermal loss. This is because that the proportional insulation thickness (and hence thermal resistance) of thinner pipes is lower per unit of mass flow, in comparison to that of thicker pipes. However, the indicator of thermal loss is nearly negligible. It merely accounts for less than 1% of the five indicators combined. This is due to the small temperature gap between the chilled water and the soil. In contrast, likewise, the impact of thermal loss on cost-effectiveness is expected to be higher in the context for district heating systems.

3.2.4. Pumps and pressure drop

The DCS cost-effectiveness indicator of pumps accounts for ~4% to ~6% of the five indicators combined, yet no obvious trends are witnessed for it with the design variables.

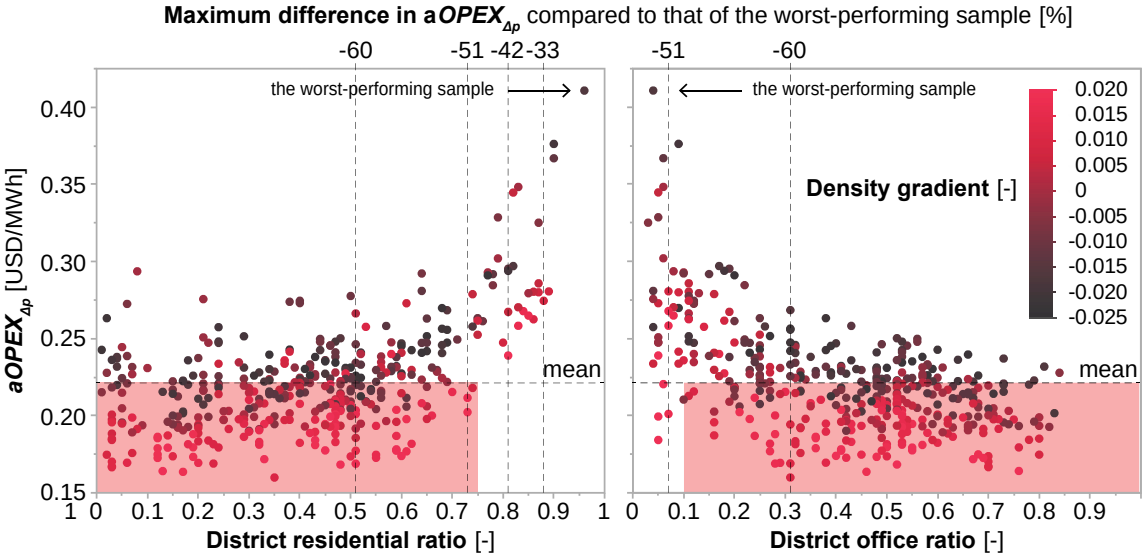

Figure 16. DCS cost-effectiveness indicator of pressure drop, denoted as $\boldsymbol{aOPEX_{\Delta p}}$ [USD/MWh] by District residential ratio [-], District office ratio [-], and the Density gradient [-].

In Figure 16, the DCS cost-effectiveness indicator of pressure drop improves as the District residential ratio decreases and District office ratio increases. This trend confirms its trade-off with the indicator of chillers and cooling towers. The rate of improvement slows down as the District residential ratio falls below ~0.75 and the District office ratio exceeds ~0.1. To explain this, we use the pipe diameters and the time of high mass flow rate. For residential-dominated samples, thinner pipes and extended hours of high mass flow rate worsen the pressure drop (Rogenhofer, 2018). Moreover, for samples with similar land use ratios, a higher Density gradient tends to improve the DCS cost-effectiveness. By having more floor area density close to the DCS cooling plant, the improvement can reach as much as ~50%. This is because samples with more floor area density further away from the DCS cooling plant have longer distances for distributing the chilled water that causes more pressure drop (Rogenhofer, 2018). The District land use ratio of the samples shaded in Figure 16 that with a high Density gradient, can potentially keep the indicator of pressure drop below its mean in the simulated dataset.

3.3. Absolute costs and overall cost-effectiveness

In **Figure 17**, the parallel plot presents the relationships between the absolute annualized capital and annual operational costs, the overall cost-effectiveness, and the district's dominant land use. Three observations are made as follows. First, the design of land uses affects both the annualized capital and annual operational costs by up to ~270% and ~180%, respectively. In general, both costs increase for samples with the dominant land use following the order of residential, office, and retail. Both the lowest annualized capital and annual operational costs are found in the sample with a District residential ratio at ~0.96. Second, low costs do not necessarily lead to high overall cost-effectiveness, and vice versa. High cost-effectiveness can be achieved through an appropriate design of land uses and is hardly relevant to the size of the absolute costs. For samples with 80th and above for the overall cost-effectiveness, the highest absolute costs are found to be ~165% and ~115% more than the cheapest annualized capital and annual operational costs, respectively. Third, decent over cost-effectiveness can be achieved regardless of the sample's dominant land use. For

samples with 60th and above for the overall cost-effectiveness, the dominant land uses are found to be any of the three, The flexibility for a mixed-use design exists, yet for a wide span of the absolute costs. However, no obvious trends can be made when the parallel plot is color-coded by the design variables related to the spatial distribution of floor area density and land uses, like Density gradient, Residential or Office gradient.

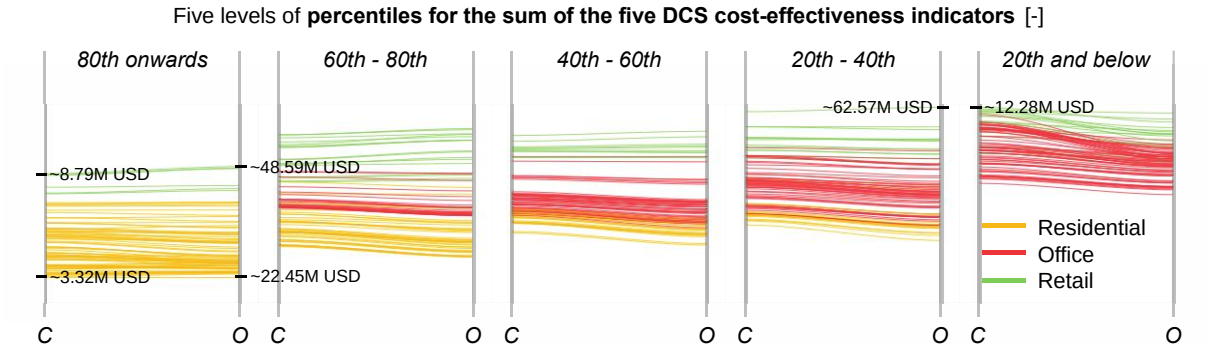

Figure 17. The annualized capital (denoted as $\boldsymbol{C}$) and annual operational (denoted as $\boldsymbol{O}$) costs [USD] grouped by five levels of percentiles for the sum of the five DCS cost-effectiveness indicators [-], color-coded by the dominant land use of residential, office, and retail [-].

4. Discussion

4.1. Land uses

4.1.1. District land use ratio

The analyses in Section 3 reveal that the District land use ratio has a more dominant role than the land use gradients on influencing the DCS cost-effectiveness as well as the absolute annualized capital and annual operational costs. For the simulated samples with the same District land use ratio, the impact of either their Residential gradient or Office gradient is witnessed to be less than 2% of the five DCS cost-effectiveness indicators combined. All these show that the District land use ratio outweighs the spatial distribution of land uses in proximity to the district cooling plant. It grants high flexibility to the urban designers for assigning the land uses for each block within the district, as long as the District land use ratio falls into a certain range.

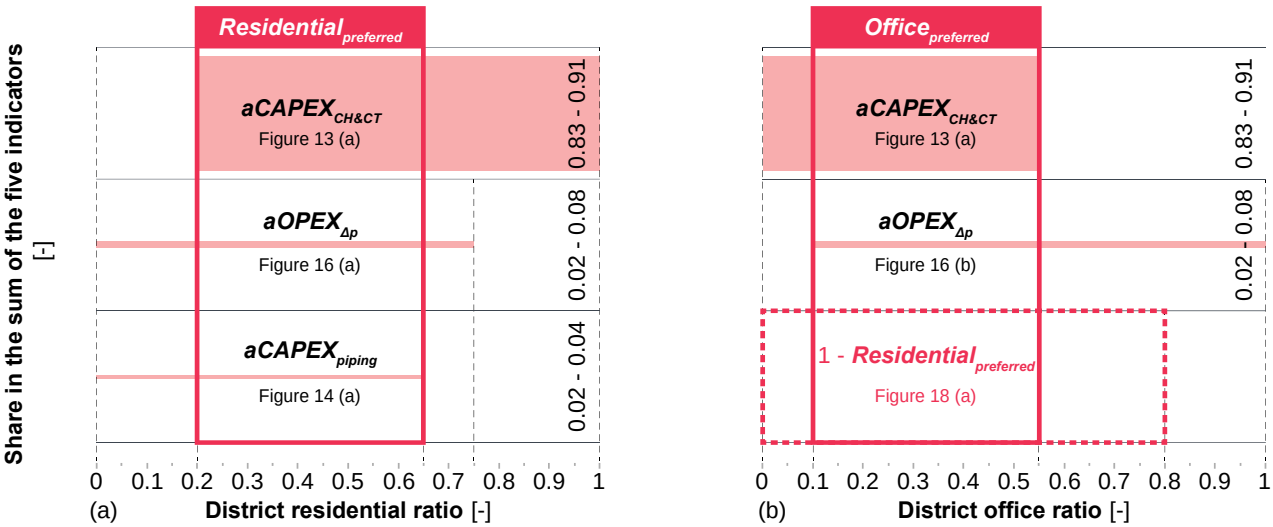

Figure 18. Constraints for the design of land uses on District residential ratio [-] and District office ratio [-] for high DCS cost-effectiveness based on the shades in Section 3.2.

Figure 18 illustrates the method we use to spot the range of District land use ratio for cost-effective DCS. We overlay the shaded range of the preferred District residential and office ratio for each DCS cost-effectiveness indicator analyzed in Section 3. For the overall preferred District residential ratio, a range between ~0.2 to ~0.65 satisfies all three relevant indicators and allows flexibility for a mixed-use design. The range for the overall preferred District office ratio is therefore set between ~0.1 to ~0.55. This range is subject to the selected District residential ratio as an addition to the two relevant indicators. However, this finding is

context-specific. A context of varied human habits, climates, locations, ratios of air-conditioned area, and building management may require different ranges of the preferred District land use ratio.

4.1.2. District residential ratio

District residential ratio, in particular, appears to be of great importance for the DCS cost-effectiveness and absolute costs. In urban design, an appropriate District residential ratio helps to achieve design goals like proximity to workplaces and all-day vitality in the public spaces, etc. However, as a matter of fact, a recent study on eight exemplary high-density districts worldwide shows that only three of the eight have a District residential ratio above 0.20 and some even have none (Christiaanse et al., 2019). Marina Bay in Singapore is one of the eight and has a District residential ratio at 0.06. Despite the advantages, the inclusion of residential to high-density districts is a decision out of factors like politics, need and supply, land price, infrastructure availability, and environmental condition, etc.

Moreover, the connection of residential land use to DCS is also subject to the game of multiple stakeholders (Gang et al., 2016). First, the sellable air-conditioner ledge of the split-units is not subject to the restriction on the floor area in Singapore. Thus, it hurts the interests of the real estate developer by connecting the residential building to DCS and removing the sellable air-conditioner ledge (Shi, Fonseca, et al., 2017a). Second, residential is not always preferred by the service providers for the fluctuating electricity prices over the 24 hours of a day. For example, in Singapore, they may produce and store the chilled water when the electricity tariff is lower at night and sell it out to other types of end-users during the peak time. Also, the occupancy schedule of residential is often versatile (Happle et al., 2017), making it difficult to predict the residents' actual need for chilled water. This adds up the risk and uncertainties for the service providers.

4.2. Floor area density

The Density gradient is able to affect the DCS cost-effectiveness indicators of piping and pressure drop by up to ~55%. A high Density gradient or keeping a high floor area density in proximity to the DCS cooling plant improves the DCS cost-effectiveness. This is in line with some other urban design strategies. For example, a transit-oriented development tends to have higher floor area density immediately next to the transit station for higher accessibility and real estate values (Cervero & Guerra, 2011). Integrating a transit station design with a DCS cooling plant underneath can maximize the usage of the public land and alleviate the conditions of land scarcity. Furthermore, the underground pedestrian tunnels connecting the buildings from the transit stations may also be integrated into the Common Service Tunnel Plan. Such integration may enhance the advantages of the common service tunnels for easy repair and maintenance, and help to justify the massive investment in a shorter term.

4.3. Limitations

The limitations of this research come in five points. (1) We use simplified building footprints by an offset of the blocks' borderlines. However, a high-density urban quarter may have various types of building footprints, like courtyards, slabs, etc. As the form of the building geometries may influence the cooling demand forecasting by affecting the received solar radiation, other types of building footprints shall be included in future studies. (2) For a mixed-use building, the HVAC inputs for the main use type are assigned to the entire building regardless of the characters of the other use types, like ratio air-conditioned area, set-point, etc. This drawback of the City Energy Analyst hurts the accuracy of cooling demand forecasting. The simulation program to be adopted in future studies should be better able to conduct the cooling demand forecasting in multiple zones for different land use types. (3) Regarding the DCS design, all the DCS components are assigned with a given technology. However, other technologies (e.g., pipes with various insulations, seawater-sourced chillers, etc.) shall be explored in future studies. (4) An artificial neural network is used to compensate for the high computing complexity for Sobol' sensitivity analysis. As the simulated dataset is small, the predicted results for the DCS indicators of pumps and pressure drop are not good enough for advising the importance of input design variables. As the computational power or the simulation tool's efficiency improves, a bigger number of simulated samples are to be expected in future similar works. (5) Concerning the various stakeholders involved in the entire process of decision-making, we mainly focus on the interests of the DCS service providers. In future studies, should the perspectives of the real estate developers and the residents are considered, heat exchangers and the intra-block chilled water distributions shall be included for the performance assessment of DCS cost-effectiveness.

5. Conclusions

This work presents an investigation on the quantified interdependencies between the design of floor area density, land uses and the cost-effectiveness of district cooling systems in high-density cities. To approach this, we integrate a parametric geometric model for urban design in Grasshopper with a detailed engineering

model of urban energy system design and assessment, named the City Energy Analyst. In building the urban design model for studying the spatial distributions of floor area density and land uses, we introduce metrics named Density gradient and Land use gradient. Two research questions are answered as follows, using Downtown Singapore as an example.

To what extent do floor area density and land use design influence the DCS cost-effectiveness? From the perspective of DCS service providers, the influence of these factors can reach ~60% to ~75% for the DCS cost-effectiveness indicators of capital costs and ~150% to ~175% for the rest on operational costs. District land use ratios, especially the District residential ratio, have the most dominant impact on the DCS cost-effectiveness, followed by the spatial distribution of floor area density. The impact of the spatial distributions of land use does exist, yet almost negligible. In addition, the indicator of chillers and cooling towers counts for up to ~83% - ~91% of the five indicators combined. It is followed by the indicators of pressure drop, piping, and pumps for ~2% - ~8% each. The indicator of thermal loss is nearly negligible for contributing to less than 1%.

At the early stage of urban design processes, how can the design of floor area density and land use help to reach better DCS cost-effectiveness? Based on our experiments and discussion throughout this study, the preferred range of the District residential ratio is between ~0.20 and ~0.65 and that of the District residential ratio is between ~0.10 and ~0.55. In general, high District residential ratio leads to an increase in the DCS cost-effectiveness and a decrease in the absolute costs. However, the inclusion of Residential land use is subject to further evaluations, acknowledging the interests of other stakeholders or the complex operating conditions (e.g., the electricity tariff differences between the day and the night). In addition, though less impactful, higher floor area density is advised to be spatially allocated in proximity to the DCS cooling plant. We hope the method and these design insights help urban planners and designers better shape high-density urban quarters serviced by district cooling systems.

Acknowledgments

References

ASHRAE Project Committee 90.1. (2019). *Schedules and internal loads for Appendix C*.

Bergman, T. L., Lavine, A. S., Incropera, F. P., & DeWitt, D. P. (2017). *Fundamentals of Heat and Mass Transfer, 8th Edition*. Wiley & Sons, Inc. https://www.wiley.com/en-us/Fundamentals+of+Heat+and+Mass+Transfer%2C+8th+Edition-p-ES81119320425

Best, R. E., Flager, F., & Lepech, M. D. (2015). Modeling and optimization of building mix and energy supply technology for urban districts. *Applied Energy*, *159*, 161–177. https://doi.org/10.1016/j.apenergy.2015.08.076

Cajot, S., Schüler, N., Peter, M., Page, J., Koch, A., & Maréchal, F. (2016). *Establishing links for the planning of sustainable districts*. Sustainable Built Environment (SBE) Regional Conference, Zurich.

Cervero, R., & Guerra, E. (2011). *Urban densities and transit: A multi-dimensional perspective*. UC Berkeley Center for Future Urban Transport. http://www.its.berkeley.edu/sites/default/files/publications/UCB/2011/VWP/UCB-ITS-VWP-2011-6.pdf

Cheng, V., Steemers, K., Montavon, M., & Compagnon, R. (2006). *Urban Form, Density and Solar Potential*. PLEA 2006. https://infoscience.epfl.ch/record/84787?ln=en

Chow, T. T., Chan, A. L. S., & Song, C. L. (2004). Building-mix optimization in district cooling system implementation. *Applied Energy*, *77*(1), 1–13. https://doi.org/10.1016/S0306-2619(03)00102-8

Christiaanse, K., Gasco, A., & Hanakata, N. (2019). *The Grand Projet: Understanding the making and impact of urban megaprojects*. nai010 publishers. https://www.nai010.com/en/publicaties/the-grand-projet/240662#xd_co_f=MmUzN2M2M2VmMWExNzRjZmFkYTE1MzM0OTMzNTg2MDg=~

Cormen, T. H., Leiserson, C. E., Rivest, R. L., & Stein, C. (2009). *Introduction to Algorithms, 3rd Edition* (3rd edition). The MIT Press.

Delgarm, N., Sajadi, B., Azarbad, K., & Delgarm, S. (2018). Sensitivity analysis of building energy performance: A simulation-based approach using OFAT and variance-based sensitivity analysis methods. *Journal of Building Engineering*, *15*, 181–193. https://doi.org/10.1016/j.jobe.2017.11.020

Energy Market Authority. (2018). *EMA : Electricity Tariffs*. https://www.ema.gov.sg/Residential_Electricity_Tariffs.aspx

Fonseca, J. A., Estévez-Mauriz, L., Forgaci, C., & Björling, N. (2017). Spatial heterogeneity for environmental performance and resilient behavior in energy and transportation systems. *Computers, Environment and Urban Systems*, *62*, 136–145. https://doi.org/10.1016/j.compenvurbsys.2016.11.001

Fonseca, J. A., Nguyen, T.-A., Schlueter, A., & Marechal, F. (2016). City Energy Analyst (CEA): Integrated framework for analysis and optimization of building energy systems in neighborhoods and city districts. *Energy and Buildings*, *113*, 202–226. https://doi.org/10.1016/j.enbuild.2015.11.055

Gang, W., Wang, S., Xiao, F., & Gao, D. (2016). District cooling systems: Technology integration, system optimization, challenges and opportunities for applications. *Renewable and Sustainable Energy Reviews*, *53*, 253–264. https://doi.org/10.1016/j.rser.2015.08.051

Guelpa, E., Toro, C., Sciacovelli, A., Melli, R., Sciubba, E., & Verda, V. (2016). Optimal operation of large district heating networks through fast fluid-dynamic simulation. *Energy*, *102*, 586–595. https://doi.org/10.1016/j.energy.2016.02.058

Happle, G., Fonseca, J. A., & Schlueter, A. (2018). A review on occupant behavior in urban building energy models. *Energy and Buildings*, *174*, 276–292. https://doi.org/10.1016/j.enbuild.2018.06.030

Happle, G., Wilhelm, E., Fonseca, J. A., & Schlueter, A. (2017). Determining air-conditioning usage patterns in Singapore from distributed, portable sensors. *Energy Procedia*, *122*, 313–318. https://doi.org/10.1016/j.egypro.2017.07.328

Herman, J., & Usher, W. (2017). SALib: An open-source Python library for Sensitivity Analysis. *Journal of Open Source Software*, *2*(9). https://doi.org/10.21105/joss.00097

Keçebaş, A., Ali Alkan, M., & Bayhan, M. (2011). Thermo-economic analysis of pipe insulation for district heating piping systems. *Applied Thermal Engineering*, *31*(17), 3929–3937. https://doi.org/10.1016/j.applthermaleng.2011.07.042

Kristensen, M. H., & Petersen, S. (2016). Choosing the appropriate sensitivity analysis method for building energy model-based investigations. *Energy and Buildings*, *130*, 166–176. https://doi.org/10.1016/j.enbuild.2016.08.038

Letellier-Duchesne, S., & Nagpal, S. (2017). *District Energy Plugin*. https://umidocs.readthedocs.io/en/latest/docs/plugins/district-energy.html#

Letellier-Duchesne, S., Nagpal, S., Kummert, M., & Reinhart, C. (2018). Balancing demand and supply: Linking neighborhood-level building load calculations with detailed district energy network analysis models. *Energy*, *150*, 913–925. https://doi.org/10.1016/j.energy.2018.02.138

Li, Y., Rezgui, Y., & Zhu, H. (2017). District heating and cooling optimization and enhancement – Towards integration of renewables, storage and smart grid. *Renewable and Sustainable Energy Reviews*, *72*(Supplement C), 281–294. https://doi.org/10.1016/j.rser.2017.01.061

Mavromatidis, G., Orehounig, K., & Carmeliet, J. (2018). Uncertainty and global sensitivity analysis for the optimal design of distributed energy systems. *Applied Energy*, *214*, 219–238. https://doi.org/10.1016/j.apenergy.2018.01.062

McCabe, R. E., Bender, J. J., & Potter, K. R. (1995). Subsurface ground temperature: Implications for a district cooling system. *ASHRAE Journal*, *37*(12). https://www.osti.gov/biblio/215474

Mohandes, S. R., Zhang, X., & Mahdiyar, A. (2019). A comprehensive review on the application of artificial neural networks in building energy analysis. *Neurocomputing*, *340*, 55–75. https://doi.org/10.1016/j.neucom.2019.02.040

Morris, M. D. (1991). Factorial Sampling Plans for Preliminary Computational Experiments. *Technometrics*, *33*(2), 161–174. JSTOR. https://doi.org/10.2307/1269043

Natanian, J., Aleksandrowicz, O., & Auer, T. (2019). A parametric approach to optimizing urban form, energy balance and environmental quality: The case of Mediterranean districts. *Applied Energy*, *254*, 113637. https://doi.org/10.1016/j.apenergy.2019.113637

Petersen, S., Kristensen, M. H., & Knudsen, M. D. (2019). Prerequisites for reliable sensitivity analysis of a high fidelity building energy model. *Energy and Buildings*, *183*, 1–16. https://doi.org/10.1016/j.enbuild.2018.10.035

Reinhart, C. F., Dogan, T., Jakubiec, J. A., Rakha, T., & Sang, A. (2013). UMI - An urban simulation environment for building energy use, daylighting and walkability. *Proceedings of BS 2013: 13th Conference of the International Building Performance Simulation Association*, *476–483*.

Robert McNeel & Associates. (2019). *Grasshopper*. https://www.grasshopper3d.com/

Rogenhofer, L. (2018). *Thermal and hydraulic modelling and optimization of thermal networks in districts in the CEA framework*. https://www.research-collection.ethz.ch/handle/20.500.11850/310828

Roudsari, M. S., & Pak, M. (2013). *Ladybug: A parametric environmental plugin for Grasshopper to help designers create an environmentally-conscious design*. 13th Conference of International Building Performance Simulation Association, Chambery, France.

Saltelli, A., Annoni, P., Azzini, I., Campolongo, F., Ratto, M., & Tarantola, S. (2010). Variance based sensitivity analysis of model output. Design and estimator for the total sensitivity index. *Computer Physics Communications*, *181*(2), 259–270. https://doi.org/10.1016/j.cpc.2009.09.018

SAS Institute Inc. (2016). *JMP 13* (Version 13) [Computer software].

Shi, Z., Fonseca, J. A., & Schlueter, A. (2017a). *Building regulations and urban policies as incentives for application of district cooling systems in Singapore*. World Sustainable Built Environment Conference 2017 Hong Kong, Hong Kong.

Shi, Z., Fonseca, J. A., & Schlueter, A. (2017b). A review of simulation-based urban form generation and optimization for energy-driven urban design. *Building and Environment*, *121*, 119–129. https://doi.org/10.1016/j.buildenv.2017.05.006

Shi, Z., Fonseca, J. A., & Schlueter, A. (2019). *Estimating the renewable energy potential with block typologies*.

Shi, Z., Hsieh, S., Sreepathi, B. K., Fonseca, J. A., & Schlueter, A. (2017). *Pilot studies on optimizing land use, building density and solar electricity generation in dense urban settings.* ISUF 2017 (the 24th International Seminar on Urban Form), Valencia, Spain.

Shmueli, G., Bruce, P. C., Stephens, M. L., & Patel, N. R. (2017). *Data Mining for Business Analytics: Concepts, Techniques, and Applications with JMP Pro*. John Wiley & Sons Inc. https://www.wiley.com/en-sg/Data+Mining+for+Business+Analytics%3A+Concepts%2C+Techniques%2C+and+Applications+with+JMP+Pro-p-9781118877432

Silva, M., Leal, V., Oliveira, V., & Horta, I. M. (2018). A scenario-based approach for assessing the energy performance of urban development pathways. *Sustainable Cities and Society*, *40*, 372–382. https://doi.org/10.1016/j.scs.2018.01.028

Sobol′, I. M. (2001). Global sensitivity indices for nonlinear mathematical models and their Monte Carlo estimates. *Mathematics and Computers in Simulation*, *55*(1), 271–280. https://doi.org/10.1016/S0378-4754(00)00270-6

The CEA team. (2019). *City Energy Analyst v2.9.2*. Zenodo. https://doi.org/10.5281/zenodo.1487867

Tian, W. (2013). A review of sensitivity analysis methods in building energy analysis. *Renewable and Sustainable Energy Reviews*, *20*, 411–419. https://doi.org/10.1016/j.rser.2012.12.014

UNEP. (2015). *District energy in cities: Unlocking the potential of energy efficiency and renewable energy*.

Urban Redevelopment Authority. (2014). *Master Plan*. https://www.ura.gov.sg/uol/master-plan.aspx?p1=view-master-plan#

Yan, C., Gang, W., Niu, X., Peng, X., & Wang, S. (2017). Quantitative evaluation of the impact of building load characteristics on energy performance of district cooling systems. *Applied Energy*, *205*, 635–643. https://doi.org/10.1016/j.apenergy.2017.08.022

Zhang, J., Xu, L., Shabunko, V., Tay, S. E. R., Sun, H., Lau, S. S. Y., & Reindl, T. (2019). Impact of urban block typology on building solar potential and energy use efficiency in tropical high-density city. *Applied Energy*, *240*, 513–533. https://doi.org/10.1016/j.apenergy.2019.02.033